

# LITHOPHYSAL POROSITY EFFECT ON MECHANICAL PROPERTIES OF WELDED TOPOPAH SPRING TUFF

L. MA<sup>1</sup> and J.J.K. DAEMEN<sup>2</sup>

<sup>1</sup>*Vector Engineering, Inc., 143E Spring Hill Drive, Grass Valley, CA 95945, USA  
(e-mail of corresponding author: ma@vectoreng.com)*

<sup>2</sup>*Department of Mining Engineering, University of Nevada, Reno, Nevada, USA*

About 81% of the proposed U.S. repository for the permanent disposal of high-level radioactive nuclear waste will be situated in the lower lithophysal unit of the welded Topopah Spring Tuff formation (Ttptll), Yucca Mountain, Nevada, and 4% will be in the upper lithophysal unit (Ttptul). Lithophysae or lithophysal cavities are a major feature in these units. The influence of the lithophysal cavities on mechanical properties of the welded tuffs was investigated. Seven cylindrical tuff specimens from Ttptll and seventeen from Ttptul were tested in uniaxial compression. Uniaxial compressive strength, Young's modulus and peak axial strain decrease with increasing lithophysal cavity content, or porosity. The relationships between strength, Young's modulus and peak axial strain versus lithophysal porosity can be best described with exponential functions. Compared to nonlithophysal tuff, failure of the lithophysal tuff specimens exhibited less brittle behavior. With an increase of porosity, the failure mode tended to be more ductile. When conducting multiple loading-unloading cycles, the maximum stress for the second and later cycles exhibited "memory" effect, i.e. the specimens "remember" the strength at the unloading point in the previous cycles before the specimens lost elasticity.

*Keywords:* Welded Tuff; Lithophysae; Lithophysal Cavities; Lithophysal Porosity; Porosity Softening; Yucca Mountain.

## 1. Introduction

A high level radioactive nuclear waste repository has been proposed to be constructed at Yucca Mountain, Nevada. Four geologic units of welded Topopah Spring Tuff formation comprise the potential repository host horizon. Units in the formation include the Topopah Spring crystal-poor upper lithophysal zone (Ttptul), the Topopah Spring crystal-poor middle nonlithophysal zone (Ttptmn), the Topopah Spring crystal-poor lower lithophysal zone (Ttptll), and the Topopah Spring crystal-poor lower nonlithophysal zone (Ttptln) (OCRWM, 1999). About 81% of the proposed repository will be situated in Ttptll and 4% in Ttptul (Islam, 2004). The lithophysae in these two units are an important feature that affects mechanical properties and other properties of the tuffs. Lithophysae or lithophysal cavities are bubble-like voids, which were formed by trapped air within the falling volcanic ash that formed the tuff units and generally are not interconnected (Avar *et al.*, 2003). In Ttptul, lithophysae generally comprise 25 to 40 percent of the tuff. Lithophysae range in size from less than 1 cm to 80 cm. In Ttptll, lithophysae vary from 3 to 30 percent of the tuff (OCRWM, 1999).

For analysis of mechanical response, lithophysae content in the welded tuffs can be treated as porosity which is defined as the ratio of volume of lithophysal voids to total specimen volume. It has been recognized that uniaxial compressive strength and Young's modulus of rocks decrease with increasing porosity. For the relation between uniaxial compressive strength and porosity, a power function was reported by Dunn *et al.* (1973) for sandstones. Exponential functions were reported by Al-Harhi *et al.* (1999) for basalt, by Vernik *et al.* (1993) for siliciclastic rocks, by Knudsen (1959) for polycrystalline specimens and by Palchik and Hatzor (2004) for porous chalks. Young's modulus as a linear function of porosity was proposed by Price (1983) and Avar *et al.* (2003) for welded Topopah Spring tuffs.

In this paper, the influence of the lithophysae on uniaxial compressive strength, Young's modulus and peak axial strain of welded Topopah Spring tuffs is investigated. It has been found that uniaxial compressive strength, Young's modulus and peak axial strain of the tuffs decrease with increasing porosity as exponential functions. As a general trend, failure mode of the tuffs transits from quasi-brittle to ductile with increasing porosity. It was observed that a memory effect exists in the tuffs when conducting multiple loading-unloading cycles.

## 2. Experimental Procedures and Results

Twenty four cylindrical tuff specimens from Tptpll and Tptpul were tested in uniaxial compression. Nineteen of them have diameter of 61 mm and five have a diameter of 83 mm. Seventeen were from Tptpul and seven from Tptpll. Table 1 gives source information, dimensions and mass of the test specimens.

Table 1. Source information, dimensions and mass of specimens.

Specimen	Borehole	Unit (zone)	Diameter (mm)	Length (mm)	Mass (g)
01014755-U	USW UZ-14	Tptpll	61	128	757
01014979-U	UE-25 UZ#16	Tptpul	61	126	702
01014985-U	USW SD-12	Tptpul	61	122	683
01014994-U	USW SD-12	Tptpul	61	118	628
01015001-U	USW SD-12	Tptpul	61	120	676
01015004-U	USW SD-12	Tptpul	61	105	617
01015455-1-U	USW SD-12	Tptpul	61	101	519
01015456-U	USW SD-12	Tptpul	61	100	577
01014723-U	UE-25-UZ#16	Tptpll	61	115	745
01014759-U	USW UZ-14	Tptpll	61	125	769
01014760-U	USW UZ-14	Tptpll	61	145	876
01014765-U	USW UZ-14	Tptpll	61	107	680
01014779-1-U	USW UZ-14	Tptpll	61	142	932
01014780-U	USW UZ-14	Tptpll	61	126	832
01014947-1-U	UE-25 UZ#16	Tptpul	61	101	615
01014977-U	UE-25 UZ#16	Tptpul	61	124	705
01014986-U	USW SD-12	Tptpul	61	99	619
01015003-U	USW SD-12	Tptpul	61	135	796
01015453-U	USW SD-12	Tptpul	61	118	697
01014911-U	USW NRG-6	Tptpul	83	160	1534
01014913-U	USW NRG-6	Tptpul	83	165	1560
01014917-1-U	USW NRG-6	Tptpul	83	153	1429
01014917-2-U	USW NRG-6	Tptpul	83	175	1680
01014923-U	USW NRG-6	Tptpul	83	150	1559

Drill cores were received from the Sample Management Facility (SMF), Yucca Mountain Site Characterization Project. Test specimens were cut from these drill cores. The ends of each specimen were ground. The specimen preparation followed ASTM D 4543. The specimens were oven-dried before testing. The average water content before drying is about 1%.

All the tests were conducted in an MTS (Material Testing System), servo-controlled hydraulic testing frame. Constant displacement rate was controlled when conducting the tests. The specimens were loaded in compression to failure within 5-10 minutes in accordance with ASTM D 2938. Load was measured using a load cell. Displacement was measured using an LVDT (linear variable differential transformer) in the MTS. Figure 1 shows a test specimen under loading. Figure 2 shows specimens before and after testing.



Fig. 1. A specimen under testing (specimen 01015453-U).



(a) 01014759-U (before test)



(b) 01014759-U (after test)



(c) 01014911-U (after test)



(d) 01015003-U (before test)



(e) 01015003-U (after test)



(f) 01014913-U (after test)

Fig. 2. Test specimens containing lithophysae (before and after test).

Due to the lithophysae, it is not possible to install strain gauges that measure an “average” strain. For only six specimens have we been able to measure strains using strain gauges and calculate some “nominal” Young’s modulus. Given that strain gauge measurements in these specimens are highly affected by lithophysae, the measurements are considered as local strains. The primary purpose of strain gauges on lithophysal specimens was to identify strain (stress) concentrations around lithophysal cavities, with the ultimate intent of trying to identify failure mechanisms, initiation to ultimate collapse. For this reason strain gauge measurements are considered somewhat suspect for the current analysis. The “nominal” Young’s moduli calculated from the strain gauge measurements are listed in Table 2 for reference only.

The LVDT measurement corresponds to total deformation in the testing system, which not only included the deformation of the tuff specimen, but also the deformations of steel platens, spacers, load cell and each contact pairs of these components. The deformation of a specimen was calculated by subtracting the deformations of all other components from the total deformation. The axial deformation of a tuff specimen  $d_{tuff}$  is calculated by

$$d_{tuff} = d_{total} - d_{system} \quad (1)$$

where  $d_{total}$  is the total deformation measured by LVDT.  $d_{system}$  is the deformations of steel platens, spacers, load cell and each contact pairs of these components. It is calculated by

$$d_{system} = F / K_{system} \quad (2)$$

where  $F$  is axial load.  $K_{system}$  is the stiffness of the system including the loading frame, steel platens, spacers and the load cell.  $K_{system}$  is obtained by loading a standard aluminum specimen, and determined by

$$\frac{1}{K_{system}} = \frac{1}{K_{total}} - \frac{1}{K_{std}} \quad (3)$$

where  $K_{std}$  is the stiffness of the standard specimen, which is known.  $K_{total}$  is the stiffness of the whole testing configuration (including the specimen), and is determined by

$$K_{total} = F / d_{total} \quad (4)$$

In order to obtain a stress-strain curve, a nonlinear regression equation for  $K_{system}$  and  $F$  was estimated from the calculated system stiffness and acquired force data. This relation takes the following form

$$K_{system} = \alpha F^\beta \quad (5)$$

where  $\alpha$  and  $\beta$  are constants.

Lithophysal porosity was calculated by

$$n = \left( 1 - \frac{\rho_d}{G_s \times \rho_w} \right) \times 100\% \quad (6)$$

where  $\rho_d$  is dry bulk density of a tuff specimen;  $G_s$  is specific gravity, 2.6;  $\rho_w$  is water density,  $1 \text{ g/cm}^3$ . The porosity calculated from Eq. (6) contains not only cavity content on the macro scale, but also conventional porosity on the micro scale.

Table 2. Summary of test results.

Specimen	Porosity, %	Uniaxial Compressive	“Nominal” Young's	Young's Modulus	
		Strength, MPa	Modulus, GPa*	Axial Peak Strain	GPa**
01014755-U	22.2	30.88	N/A	0.0030	11.98
01014979-U	26.6	25.73	N/A	0.0019	13.83
01014985-U	26.5	12.01	N/A	0.0023	8.76
01014994-U	30.0	25.74	N/A	0.0022	12.07
01015001-U	26.0	15.43	N/A	0.0033	8.45
01015004-U	22.2	41.27	N/A	0.0034	18.39
01015455-1-U	32.4	18.89	N/A	0.0023	8.71
01015456-U	23.6	39.49	N/A	0.0037	16.24
01014723-U	14.9	98.80	25.73	0.0048	28.91
01014759-U	19.2	58.54	N/A	0.0038	19.31
01014760-U	20.5	44.02	20.91	0.0033	19.86
01014765-U	16.2	57.11	N/A	0.0043	16.21
01014779-1-U	13.5	92.94	22.77	0.0052	22.45
01014780-U	12.8	94.31	N/A	0.0048	28.82
01014947-1-U	19.9	49.55	29.59	0.0036	17.50
01014977-U	25.0	30.97	N/A	0.0031	13.02
01014986-U	17.9	75.70	26.03	0.0047	19.99
01015003-U	22.5	30.96	28.29	0.0025	16.75
01015453-U	22.2	33.03	N/A	0.0031	16.59
01014911-U	31.9	22.30	N/A	0.0027	11.49
01014913-U	32.9	16.14	N/A	0.0025	9.34
01014917-1-U	33.8	16.73	N/A	0.0029	8.38
01014917-2-U	31.7	22.05	N/A	0.0030	10.11
01014923-U	26.3	17.26	N/A	0.0027	10.25

\* Calculated from strain gauge measurement;

\*\* Calculated from stiffness calculation procedure, LVDT measurements.

### 3. Observations and Analysis

#### 3.1. Porosity Dependency of Uniaxial Compressive Strength

The uniaxial compressive strength is plotted against lithophysal porosity in Figure 3 for all the tests. The strength decreases with increasing porosity. This relation is best described with an exponential function as given in Eq. (7).

$$\sigma_c = 368e^{-10.1n} \quad (7)$$

Eq. (7) was estimated using nonlinear regression in the Excel SOLVER of Microsoft Office. The constants in the equation were estimated by maximizing the Pseudo-R-square, the ratio of the

regression sum of squares to the total sum of squares. This ratio explains the proportion of variance accounted for in the dependent variable by the model. It is equivalent to the R-square in linear regression. The Pseudo-R-square for Eq. (7) is 0.93.

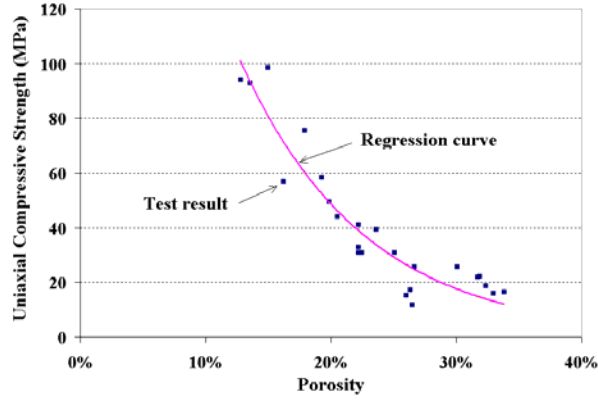


Fig. 3. Uniaxial compressive strength as an exponential function of lithophysal porosity.

In Eq. (7), when  $n = 0$ ,  $\sigma_c = 368$  MPa, which does not really exist for the tuffs. Voids in micro scale are always contained in the Topopah Spring tuffs. The authors have found that the average uniaxial compressive strength for intact nonlithophysal tuff in Ttpm under the same loading rate is 229.6 MPa (Ma *et al.*, 2006). When  $n \rightarrow 100\%$ ,  $\sigma_c \rightarrow 0$ . Sensitivity of  $\sigma_c$  to  $n$  can be expressed as  $S(\sigma_c, n)$ , and calculated by Eq. (8). It is interpreted that an increase of 1% of  $n$  leads to a 10.1% decrease of  $\sigma_c$ .

$$S(\sigma_c, n) = \frac{d\sigma_c}{dn} \times \frac{n}{\sigma_c} = -10.1n \quad (8)$$

### 3.2. Porosity Dependency of Young's Modulus

Young's modulus for this analysis was calculated at about 50% of the axial stress-strain curve using linear fitting in terms of ASTM D-3148. Calculation of axial strain was from  $d_{tuff}$  determined in Eq. (1). The plot of Young's modulus versus lithophysal porosity is shown in Figure 4. The regression analysis gives a similar relationship as between strength and lithophysal porosity. Eq. (9) is the regression equation. The Pseudo-R-square for it is 0.91. When  $n = 0$ ,  $E = 54.5$  GPa. An increase of 1% of  $n$  leads to a 5.6% decrease of  $E$ . The average Young's modulus for nonlithophysal tuff in Ttpm under the same loading rate is about 35 GPa (Ma and Daemen, 2006).

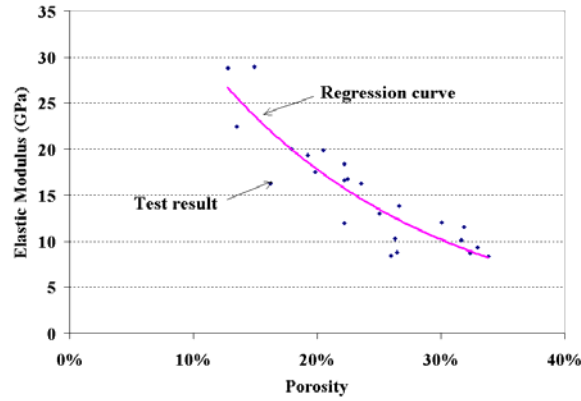


Fig. 4. Young's modulus as an exponential function of lithophysal porosity.

$$E = 54.5e^{-5.6n} \quad (9)$$

### 3.3. Porosity Dependency of Peak Axial Strain

Peak axial strain was calculated from the maximum  $d_{tuff}$  divided by the specimen length at peak stress. Porosity dependency of peak axial strain is shown in Figure 5. A regression curve in exponential form is also plotted. Eq. (10) is the regression equation with a Pseudo-R-square 0.99. When  $n = 0$ ,  $\varepsilon_{peak} = 0.008$ . An increase of 1% of  $n$  leads to a 3.94% decrease of  $\varepsilon_{peak}$ . It has been reported by the authors that the peak axial strain for nonlithophysal tuff in Tptpmn under the same loading rate is 0.006 mm/mm (Ma and Daemen, 2006).

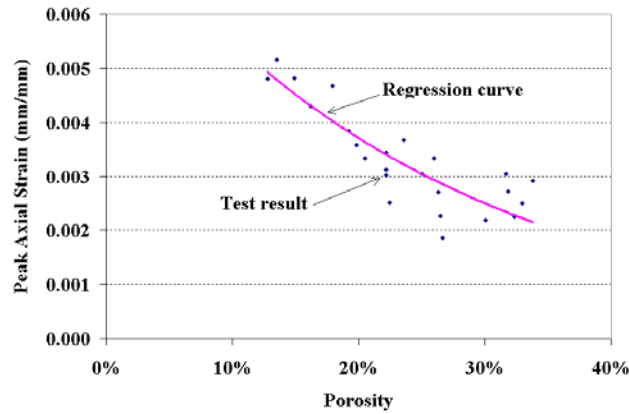


Fig. 5. Peak axial strain as an exponential function of lithophysal porosity.

$$\varepsilon_{peak} = 0.008e^{-3.94n} \quad (10)$$

In fact the exponential relation can be recognized from Eqs. (7) and (9) in terms of the relationship of  $\sigma = E\varepsilon$ , where  $\sigma$  is axial stress and  $\varepsilon$  axial strain.

### 3.4. Failure Mode and Porosity Softening

Compared to nonlithophysal tuff in Tptpmn, the failure mode of low porosity lithophysal tuffs was less brittle (Ma and Daemen, 2004). It can be defined as quasi-brittle for easy description. As a general trend, the lithophysal tuffs fail in quasi-brittle mode at low porosity, and tend to be more ductile with an increase of porosity. As described in Eqs 5, 6 and 7, uniaxial compressive strength, Young's modulus and peak axial strain decrease with increasing porosity. Based on these relations, a conceptual diagram for stress-strain relation under the variation of porosity can be constructed as shown Figure 6. With an increase of porosity, a specimen gets to "soften". This behavior can be called porosity softening.

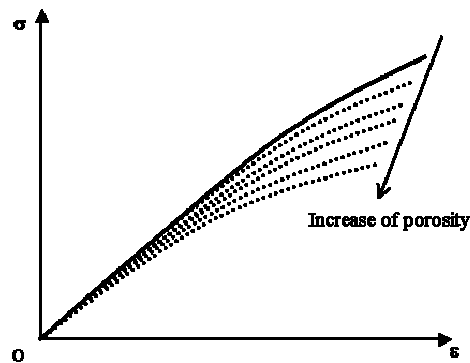


Fig. 6. Diagram for stress-strain relations under variation of porosity.

### 3.5. Memory Effect and Brittle – Ductile Transition under Multiple Loading-Unloading Cycles

Rocks are classified either as brittle or ductile. Ductility is generally acknowledged to be the result of homogeneous flow. The criteria for identifying ductility are often linked to stress-strain data (Scott and Nielsen, 1991). Byerlee (1968) defined ductility in a rock as deformation without loss of compressive strength. The brittle-ductile transition in rocks is accompanied by inelastic compaction (Scott and Nielsen, 1991).

After initial failure, the lithophysal tuffs do not completely break apart, as distinguished from the nonlithophysal tuff which typically totally disintegrate, violently (Ma and Daemen, 2004; Ma and Daemen, 2006). They tend to retain considerable residual strength. Figure 7 shows examples of stress-displacement curves of specimens that experienced multiple loading-unloading cycles. The observations from these plots can be summarized as: 1) the significant nonlinear stress-displacement relation during loading indicates a large nonlinear compression of the specimen; 2) for the second cycle (Figure 7, a and b) or later cycles (Figure 7, b) the "peak" stress (or at least a fairly large stress fairly close to the maximum) can be sustained over a large strain range. Specimens tend to be more ductile; 3) the maximum stress for any subsequent cycle is lower but close to the unloading level of the previous cycle. The rock "memorizes" its previous strength at the unloading point. This memory effect decreases with increasing loading-unloading cycles; 4) when the specimen is unloaded to zero stress, a significant strain remains as a permanent deformation; 5) significant residual strength remains even after very large deformation. The permanent deformation increases significantly with each loading-unloading cycle.

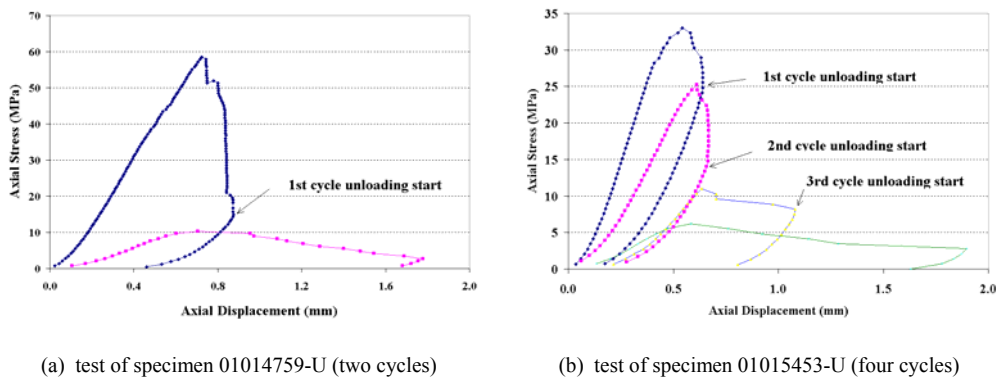


Fig. 7. Plots of stress versus total displacement.

#### 4. Conclusions

- Uniaxial compressive strength, Young's modulus and peak axial strain of lithophysal tuffs decrease with increasing lithophysal porosity following exponential functions.
- Lithophysal tuffs exhibit porosity softening and brittle-ductile transition with increasing loading-unloading cycles.
- Lithophysal tuffs "memorize" the previous strength at the unloading point when conducting multiple loading-unloading.

#### References

- Al-Harhi, A.A., Al-Amri, R.M., and Shehata, W.M. (1999). "The Porosity and Engineering Properties of Vesicular Basalt in Saudi Arabia", *Engineering Geology*, **54**: 313–320.
- ASTM D 2938-95. "Standard Test Method for Unconfined Compressive Strength of Intact Rock Core Specimens", *Annual Book of ASTM Standards*, Sec. 4, Construction, Vol. 04.08, Soil and Rock, Building Stones. American Society for Testing and Materials, Conshohocken, PA.
- ASTM D3148-02. "Standard Test Method for Elastic Moduli of Intact Rock Core Specimens in Uniaxial Compression", *Annual Book of ASTM Standards*, Sec. 4, Construction, Vol. 04.08, Soil and Rock, Building Stones. American Society for Testing and Materials, Conshohocken, PA.
- ASTM D 4543-85 (Reapproved 1991). "Standard Practice for Preparing Rock Core Specimens and Determining Dimensional and Shape Tolerances", *Annual Book of ASTM Standards*, Sec. 4, Construction, Vol. 04.08, Soil and Rock, Building Stones. American Society for Testing and Materials, Conshohocken, PA.
- Avar, B.B. (2003). "The Influence of Lithophysal Porosity on the in-situ Stress-Strain Properties of Topopah Spring Tuff", Final Technical Report, U.S. DOE/UCCSN Cooperative Agreement. DE-FC28-98NV12081. Task 27. PDF available at <http://hrcweb.lv-hrc.nevada.edu/qa/Report/TR-02-008.pdf>.
- Byerlee, J.D. (1968). "Brittle-Ductile Transition in Rocks", *J. Geophys. Res.*, **73**(14): 4741–4750.
- Dunn, D.E., LaFountain, L.J., and Jackson, R.E. (1973). "Porosity Dependence and Mechanism of Brittle Fracture in Sandstones", *J. Geophys. Res.*, **78**(14): 2403–2417.
- Islam, M. (2004). "Influence of Lithophysae Geometry and Distribution on Mechanical Properties of Topopah Spring Tuff", University and Community College System of Nevada (UCCSN)

Scientific Investigation Plan. PDF available at <http://hrcweb.nevada.edu/qa/SIP/SIP-033D1.pdf>.

- Knudsen, F.P. (1959). "Dependence of Mechanical Strength of Brittle Polycrystalline Specimens on Porosity and grain size", *Journal of the American Ceramic Society*, **42**(8): 376–387.
- Ma, L. and Daemen, J.J.K. (2006). "Strain Rate Dependent Strength and Stress-Strain Characteristics of a Welded Tuff", *Bull. Eng. Geol.Env.*, PDF available at <http://dx.doi.org/10.1007/s10064-005-0038-6>.
- Ma, L., Zhao, G., Sunkara, A. and Daemen, J. J. K. (2006). "Stress Rate Dependent Strength of a Welded Tuff in Triaxial Tests", Proceedings, 41<sup>th</sup> U.S. Rock Mechanics Symposium, Golder, Colorado, June 2006.
- Ma, L. and Daemen, J.J.K., (2004). "Time Dependent Mechanical Behavior of Welded Tuff", Final Technical Report, Prepared for U.S. DOE/UCCSN Cooperative Agreement DE-FC28-98NV12081. PDF available at <http://hrcweb.lv-hrc.nevada.edu/qa/Report/TR-03-018-2.pdf>.
- OCRWM (Office of Civilian Radioactive Waste Management) (1999). "Geology of the ECRB Cross Drift - Exploratory Studies Facility, Yucca Mountain Project, Yucca Mountain, Nevada", Prepared by Mongano, G.S., Singleton, W.L., Moyer, T.C., Beason, S.C., Eatman, G.L.W., Albin, A.L., and Lung, R.C., Bureau of Reclamation and U.S. Geological Survey. Denver, CO. Available at [http://www.ocrwm.doe.gov/documents/spg42gm3\\_a/index.htm](http://www.ocrwm.doe.gov/documents/spg42gm3_a/index.htm).
- Palchik, V. and Hatzor, Y.H. (2004). "The Influence of Porosity on Tensile and Compressive Strength of Porous Chalks", *Rock Mech. Rock Engng*, **37**(4): 331-341.
- Price, R.H. (1983). "Analysis of Rock Mechanics Properties of Volcanic Tuff Units from Yucca Mountain, Nevada Test Site", Sandia National Laboratories Report, SAND82-1315.
- Scott, T.E. and Nielsen, K.C. (1991). "The Effect of Porosity on the Brittle-Ductile Transition in Sandstones", *J. Geophys. Res.*, **96**(B1): 405-414.
- Vernik, L., Bruno, M., and Bovberg, C. (1993). Empirical relations between compressive strength and porosity of siliciclastic rocks. *Int. J. Rock Mech. & Min. Sci. Geomech. Abstr.*, **30**(7): 677–680.

### **Acknowledgements**

We thank Mr. Jaime Gonzalez, DOE Contract Manager. We thank Messrs. Rick Blitz and John Leland for experimental work. The work reported on here was partially supported through DOE Cooperative Agreement DE-FC28-04RW12232.

This paper was prepared by University of Nevada, Reno pursuant to a cooperative agreement fully funded by the United States Department of Energy, and neither University and Community College System of Nevada nor any of its contractors or subcontractors nor the United States Department of Energy, nor any person acting on behalf of either: (a) Makes any warranty or representation, express or implied, with respect to the accuracy, completeness, or usefulness of the information contained in this report, or that the use of any information, apparatus, method, or process disclosed in this report may not infringe privately-owned rights; or (b) Assumes any liabilities with respect to the use of, or for damages resulting from the use of, any information, apparatus, method or process disclosed in this report. Reference herein to any specific commercial product, process, or service by trade name, trademark, manufacturer, or otherwise, does not necessarily constitute or imply its endorsement, recommendation, or favoring by the United States Department of Energy. The views and opinions of authors expressed herein do not necessarily state or reflect those of the United States Department of Energy.